Simultaneous specimen current and time-dependent cathodoluminescence measurements on gallium nitride

Campo, Eva; Hopkins, Lauren; Pophristic, M.; Ferguson, T.

Journal of Applied Physics

DOI:
10.1063/1.4954685

Published: 28/06/2016

Peer reviewed version

Simultaneous Specimen Current and Time-Dependent Cathodoluminescence Measurements on Gallium Nitride.

E. M. Campo[1a)], L. Hopkins[1], M. Pophristic[2], and I. T. Ferguson[3]

[1] *School of Electronic Engineering, Bangor University, Gwynedd, LL57 1UT, UK*

[2] *University of the Science, Department of Chemistry and Biochemistry, Philadelphia, Pennsylvania, USA*

[3] *Department of Electrical and Computer Engineering, Missouri University of Science and Technology, Rolla, Missouri, 65409, USA*

Time-dependent cathodoluminescence (CL) and specimen current (SC) are monitored to evaluate trapping behaviour and evolution of charge storage. Examination of CL and SC suggests that the near band edge emission in GaN is reduced primarily by the activation of traps upon irradiation, and Gallium vacancies are prime candidates. At the steady state, measurement of the stored charge by empiric-analytical methods, suggests that all available traps within the interaction volume have been filled, and that additional charge is being stored interstitially, necessarily beyond the interaction volume. Once established, the space charge region is responsible for the steady state CL emission and prior to build up, it is responsible for the generation of diffusion currents. Since the non-recombination effects resulting from diffusion currents that develop early on are analogous to those leading to device failure upon aging, this study is fundamental towards a holistic insight into optical properties in GaN.

I. INTRODUCTION:

The dynamics behind electrical stress that results in optical malfunction and failure remain unresolved despite the urgency to determine mechanisms leading to electronically fatigue-resilient GaN devices.[1] Similarly, the study of charging mechanisms upon electron beam bombardment in poorly conductive materials is an active field of research.[2] And in fact, a grounded stage in an electron microscope can serve as a simulation platform, where prolonged irradiation by electron beams promote device aging and simultaneous and *in-situ* cathodoluminescence (CL) monitors impact from the inflicted electrical stress on optical properties.[3,4] This is achieved by selecting current densities in the electron beam analogous to operational currents in nitride-based laser diode devices,[5] which is conducive to the CL dynamics elucidation of aging and breakdown. In this scheme, understanding electron beam derived charging mechanisms will enable improved device operation, as it offers qualitative insight into operational aging in GaN.

---

a) Author to whom correspondence should be addressed. Electronic mail: e.campo@bangor.ac.uk

A variety of conductivity values have been reported for gallium nitride (GaN) materials, depending on carrier concentration and mobility. Carrier concentrations had been shown earlier to vary from $3x10^{16}$ to $7x10^{15}$ cm^{-2} leading to resistivity at room temperature in nominally undoped MOCVD GaN varying between 0.23 and 0.99 Ωcm, (with electron mobilities of 900 cm^2Vs^{-1}).[6] More recently, carrier concentrations below $1x10^{15}$ cm^{-2} have been reported.[7] Moreover, nitridation times of the substrate have also an impact on morphology of GaN-thin films,[8] which leads to alterations in electrical properties. Overall, the wurtzite-crystal structure of GaN bears many defects in the windows of lateral epitaxial overgrown (LEO) samples (which we are studying here), as a consequence of lattice mismatch and threading dislocation densities are known to differ by two or three orders of magnitude between window and LEO regions.[6] It is precisely the strain induced by lattice mismatch that causes defect densities of up to 10^{10} cm^{-2}, mostly arising from threading dislocations (TDs).[9] Dislocations are a source of non-radiative recombination centres, and they have been shown to act as deep donors in n-GaN and as deep acceptors in p-type GaN.[9]

The role of point defects in charge trapping remains unclear, with gallium vacancies (V_{Ga}) having the lowest formation energy of expected vacancies. In addition, formation energies of V_{Ga} and associated complexes are much smaller at sites near TDs than in the bulk.[9] In addition, V_{Ga} have been argued to be trapped in the stress fields of TDs,[9] preventing electromigration, as will be discussed later. However, TDs have also been correlated with enhanced diffusion processes to promote device degradation.[3] The abundance of V_{Ga} has prompted the tentative assignment of a number of radiative and non-radiative luminescence in GaN. Indeed, V_{Ga} were originally correlated with the origin of deep level (DL) yellow emission,[10] now attributed to C_N complexes through density functional theory calculations.[11] More recently, V_{Ga} have recently been identified as the likely cause of Near Band Edge (NBE)-CL quenching, [5,12] and in fact CL monitoring clearly identified stressed regions in operational laser diodes. Indeed, Nykänen *et al.* recently correlated reduction in photoluminescence (PL) intensity with increased concentration of V_{Ga} upon irradiation.[5] Beam energies involved were far too low to promote the removal of Ga (500 keV) or N (150 keV) from the lattice, which concluded increased defects were in fact, activated sites out of in-grown defects already existing within the bulk. Hydrogenated vacancies have ben thoroughly studied and it is well established that hydrogenated vacancies have lower formation energies than V_{Ga}.[9]

On those lines, V_{Ga}-H_3 is stable enough to exist in GaN grown by MOCVD in large concentrations, (>10^{17} cm^{-3}) as both NH_3 and TMGa provide a hydrogen source. Although earlier studies suggested that dissociation of hydrogenated V_{Ga} was unlikely,[9] it has been recently estimated that1 eV is required to remove 1H from this complex. Removal of one, two or all hydrogen atoms by an electron beam is energetically feasible and would result in the creation of deep acceptor sites acting as non-radiative recombination centers.[5,12]

It is worth highlighting that the study of electric fields in insulators is a vibrant field of research.[13] Indeed, electric fields generated in insulators and semiconductors can cause modifications in secondary electron (SE) and back scattered electron (BSE) yields,[14] even during electron beam irradiation in a low pressure SEM.[15] It has previously been shown that absorption of species to the surface can modify band bending and interfacial space charge regions.[14] In addition, charging of insulators during electron beam irradiation can lead to x-ray microanalysis artefacts[16] and to electromigration of point defects.[17]

Prior works had not considered the effects of electric fields (resulting from prolonged irradiation) on CL signal evolution to enable a distinction between stopping power processes and current density effects. In this work, simultaneous measurements of NBE CL and specimen current (SC) were conducted as a platform to visualize the interplay of optical properties based on diffusion and leakage currents, the former, believed to be responsible of ultimate failure in operational devices.[3,5,14] Earlier work had confirmed that deep level (DL) emissions remained unaffected,[14] and that surficial carbonaceous impurities were not responsible for decreased NBE signals.[18] In this study, only NBE emissions were monitored from the window regions in LEO GaN films; knowingly, where architected devices down perform those built on the LEO regions.[6] Therefore, a distinctive electro-optical pattern is expected here, that highlights the mechanisms responsible for device failure. Indeed, our momentary current density (i.e. beam flux) is on the order o of 100-200 kA/cm^2, comparable to Nykanen's (0-130 kA/cm^2) and hence to current densities in nitride laser diodes.[5] Building up the work by Nykanen *et al*., we explain the temporal evolution of NBE CL as a function of both defect activation and electric field effects.

Under the experimental conditions described here, electron beam bombardment can promote the activation of defects in GaN.[5] In addition, in this work, we will be considering direct and indirect effects from electron beam bombardment *through stored charge* on CL. By direct effects, we refer to those phenomena affecting e-h generation rate and recombination efficiency, through internal built-in fields. Indirect effects refer to electric field-induced electromigration as well as to activation of defects, beyond the activation through knock-on damage from the

electron beam. It is through a combination of the phenomena described here that device failure is expected to occur- albeit- in the active AlGaN/InGaN layers in operational GaN devices.[19] The study of these phenomena in the window regions of LEO-GaN as a model system reflects the complexity behind accurate luminescence and electrical measurements to propose a self-consistent phenomenologistic model that can be built upon for ternary systems.

Indeed, previous works examining mechanisms for electrical degradation of GaN HEMTs[20] and LEDs[21] highlight the evidence of defect formation in the active layers. In particular, Meneghini cites a decrease in internal quantum efficiency due to the generation of nonradiative centers as well as changes in the processes responsible for the injection of carriers in the active region of the devices.[21] The discussion in this manuscript addresses decreased NBE emissions in relation with the generation of defects and of a space charge region from a materials perspective; both in resonance with the phenomena described above from a device perspective. This work is relevant to those models in two ways. First, by examining the electrical behavior of the LEO grown GaN that would be connected to one of the electrodes, hence, modulating the charge and current dynamics prior to reaching the active layer. Second, by establishing a baseline describing the behavior of a chemically simpler structure than the InGaN/GaN QWs in LEDS and the AlGaN in HEMTs; whose charging/luminescence behavior will likely be more complex. An initial study of an untreated GaN epilayer within the LEO region of high dislocation is the ideal platform prior to investigating InGaN/GaN QWs and AlGaN.

In addition, a recent review by the Nakamura team highlights the current value of LEO GaN substrates,[22] and its current use in the fabrication of GaN-LDs, given the lack of suitably large HVPE freestanding substrates at present. More recently, variations of LEO growth have provided high quality coalescence through the wafer,[23] and industrial laboratories have achieved continuous wave operation of high power vertical cavity surface emitting lasers using LEO GaN.[24] It is also worth stressing that this work is important for showing the need for lower defect LEO GaN in large area substrates, in agreement with works by Song *et al*.[25]

A variety of methods have been proposed to measure charge injection in insulators during electron beam irradiation, and a brief review is included in the Supplementary Material (SM). In this work, we will use the experimental and theoretical approach devised by Song *et al*.[26] which is also described in the SM. Through this methodology, *in situ* specimen current monitoring during electron beam irradiation allows the calculation of stored charge and time constants associated with the space charge region set up. In addition, systematic variation of experimental parameters in this work (beam energy, current, and magnification) has enabled the definition of

parametric equations to estimate NBE CL time constants and to predict the steady state NBE CL emission. Finally, a model that involves the prevalence of V_{Ga} charge trapping over additional space charge region-build up or electromigration mechanisms is derived to explain the decreased time-dependent NBE CL in GaN.

II. EXPERIMENTAL

CL measurements were conducted at room temperature in a JEOL JSM-6400 SEM, equipped with a tungsten source and an Oxford Instruments CF302 CL system with parabolic mirror light collecting optics, computer-controlled SPEX 340S spectrometer, and a Hamamamtsu-R928 GaAs PMT. Output from photo multiplier tube (PMT) can be used either to acquire CL spectra by measuring CL intensity at different wavelengths (wavelength scans), to measure CL intensity at a particular wavelength through time dependent CL (t-CL), or to form monochromatic CL images. A Gatan Digiscan unit acquired SE and CL images digitally. A Keithley 427 current amplifier was connected between the specimen stage and the grounding system to measure SC as a function of time.

A nominally undoped GaN film was grown by metal organic chemical vapor deposition (MOCVD) in an Emcore Spectrablue reactor at Emcore Corp. LEO-GaN on sapphire growth used a 9 μm wide window, 100 nm thick SiN_x mask and a 2 μm thick GaN buffer layer at 1050 ˚C and 50 Torr. GaN was then grown in the window regions with lateral overgrowth over adjacent regions of the mask. The LEO film was grown with a 2 μm base layer thickness, under 25 Torr growth pressure, 0.8 μm /hr growth rate, and 1000 ˚C growth temperature. Properties of window and laterally grown area differ greatly in impurity and defect density.[6,27] A 50 Å gold-palladium (Au-Pd) coating layer was sputter-coated on the GaN surface to minimize charging effects, and electrical contact was made from the coating layer to the sample holder by conductive carbon tape. In this scheme, with one single contact from the stage to the current amplifier, the specimen current is measured, rather than an electron beam induced current or EBIC. Electron beam irradiation was performed through the Au-Pd contacts, and both CL and SC measurements were acquired. The Au-Pd coating was a continuous film, which avoided leakage current effects at the edges.

Magnification was chosen to be 15 kx, 30 kx, 60 kx, and 120 kx, with the beam in super rapid (SR) scanning mode, which is approximately half the speed of TV scanning rates. SR scanning mode improves the precision of the scanned region by minimizing over scanning which occurs for faster scanning speeds. In SEM images of the cross-section, (not shown) window width is about 9.3 μm and irradiation scan is no larger than 4.7 μm wide by 3.2 μm high at 15kx magnification; i.e. these irradiation experiments are being conducted on the window region exclusively,

which were irradiated from the top. Electron beam energy was 10 keV or 20 keV and electron beam current was 10, 15 or 20 nA. As stated earlier, in this work, the beam flux, or momentary current density varied between 100 and 200 kA/cm^2 and the beam dose or fluence ranged from 1x10^{10} to 6x10^7 μC/cm^2 .

Spectrometer slits were 8 mm for all experiments and the spectral resolution was 0.15 nm. In addition, working distance in the microscope was constant for all experiments in order to keep collection efficiency constant. Time-dependent near band edge cathodoluminescence (NBE t-CL) intensity and specimen current (SC) were acquired simultaneously in all cases. Fresh areas were scanned for each different magnification, beam current and beam energies. The sample was kept under vacuum for over 24 hours to allow desorption of any residual humidity which may affect charge carrier dynamics.[14,28] Spot mode irradiation experiments (not shown) were conducted to test homogeneity of the surface coating, conductivity was found to be consistent within irradiated regions and SC measurements were repeatable in their kinetics. All fitting parameters were found using commercial software ORIGIN.

III. RESULTS AND DISCUSSION

Wavelength scans on window regions of the sample before long-time irradiation, revealed a narrow NBE peak at approximately 370 nm and a wide deep level (DL) peak at 570 nm, as shown in Fig. 1. The reduced raster RD2 beam mode on the microscope ensured that only window regions were irradiated even at the lowest magnification. Wavelength scans after irradiation did not show emissions other than NBE and DL. Moreover, intensity of NBE was decreased after irradiation, in good agreement with time-based CL scans. Intensities of deep level emissions were not changed, as shown in SM.

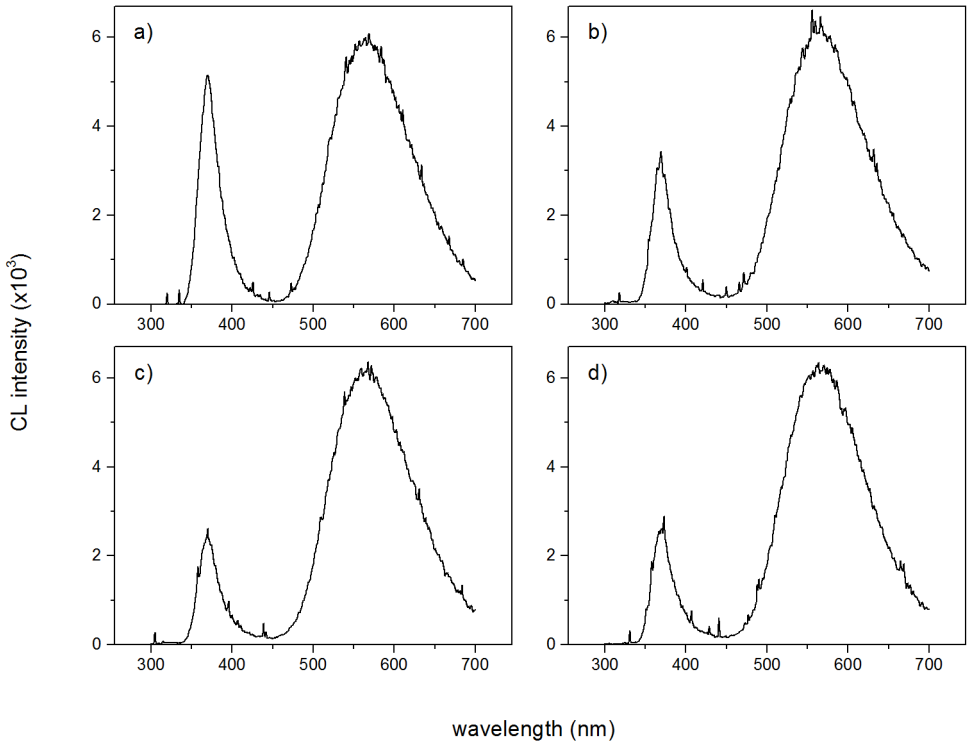

FIG.1 Wavelength scans Wavelength scans performed at 10keV 15 nA on the window regions of sample #1 at (a) 15kx magnification, (b) 30kx magnification, (c) 60kx magnification, and (d) 120kx magnification.

CL irradiation experiments were reproducible, as confirmed by multiple acquisitions. For identical irradiation conditions, scans performed in similar regions which were not previously irradiated showed that initial CL intensity in scans varied by approximately 10 % from region to region, and time constants associated with the decrease with time varied within a 2% range. CL-time based scans at the NBE wavelength are shown in Fig.2. Fig.2(a) shows CL scans for different magnifications and different beam currents with 10 keV beam voltage, Fig.1(b) shows associated in-situ SC measurements. Likewise, Fig.2(c) and (d) shows CL and SC measurements, respectively, for each experimental set up at 20 keV. All values have been normalized. SC and CL curves were smooth in most cases, but SC curves in the 20 kV experiments, Fig.2(d), showed some steps as large as 0.2 nA, possibly from temporary voltage flashover.

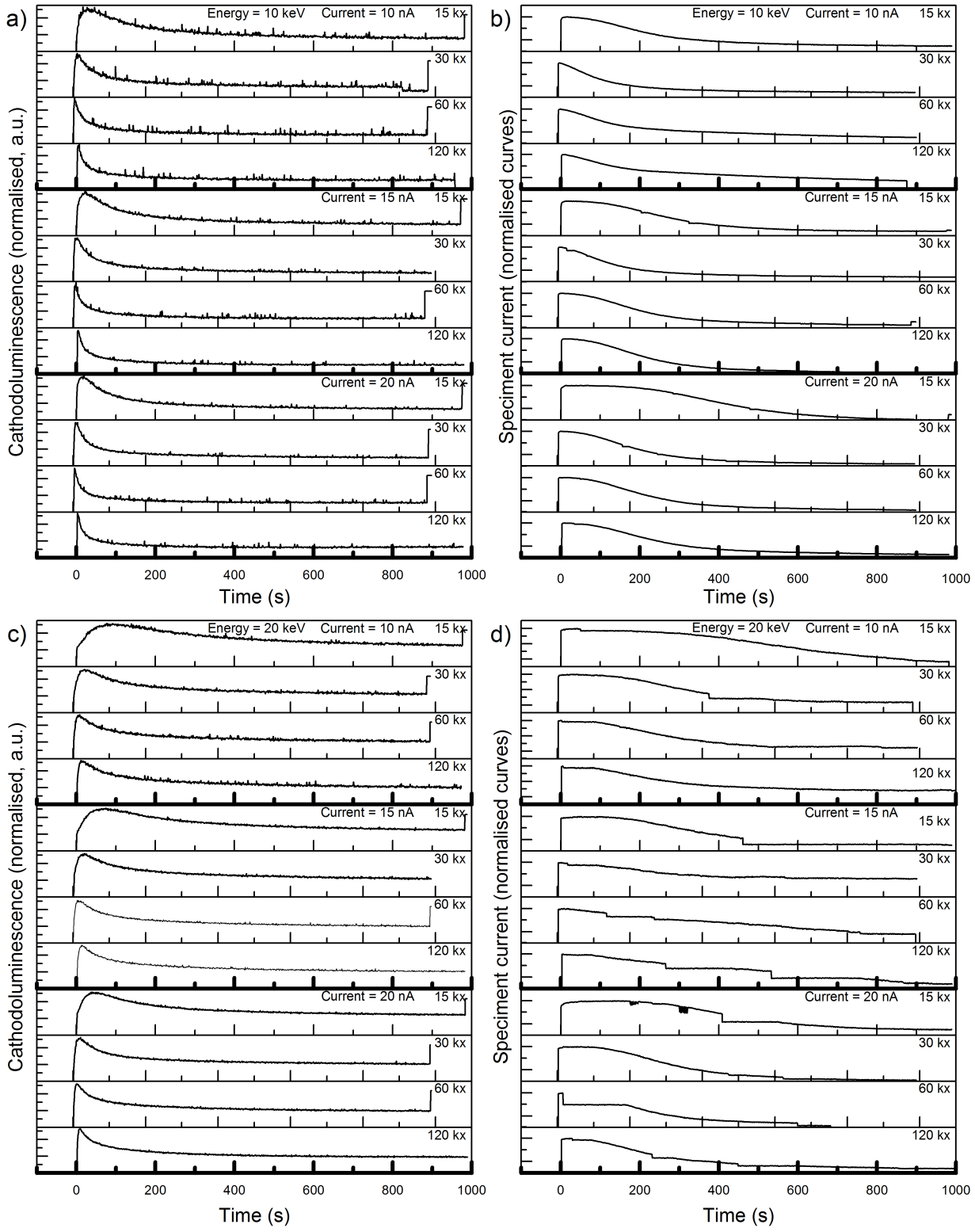

FIG. 2(a) NBE CL and (b) SC evolution at 10, 15 and 20 nA beam current for varying magnifications at beam energy of 10 keV (c) NBE CL and (d) SC evolution at 20 keV beam energy.

A. Conservation of Charge and Estimation of Interaction Volume

The stored charge was calculated from the specimen current data and from conservation of charge using a method described by Song *et al*.[26] (SM). The incident current i_o equals the sum of backscattered and secondary electron currents i_{bs} and specimen current i_{sc}.

$$i_o = i_{bs} + i_{sc} \tag{1}$$

The specimen current has two contributions, the displacement current i_d and the leakage current i_l, now;

$$i_o = i_{bs} + i_d + i_l \tag{2}$$

However, the component of specimen current related to trapped charge Q(t) is the displacement current i_d,

$$Q(\infty) = \int_0^\infty i_d(t)dt = \int_0^\infty \frac{Q(\infty)}{\tau'} e^{-t/\tau_{SC}} \cdot dt \tag{3}$$

where Q(∞) is stored charge at steady state SC and τ_{SC} a time constant associated with SC evolution.

Interaction volume depth can be analized using the Kanaya-Okayama method[29], where for a beam tilt of 0˚, the incident energy from the beam is being deposited over a volume whose radii is approximated by R_{KO}; the Kanaya-Okayama electron range:

$$R_{KO} = \frac{27.6 \cdot A \cdot E_0^{1.67}}{Z^{.89} \cdot \rho} \tag{4}$$

where, A is atomic weight in gm mol^{-1}, E_0 is beam energy in keV, Z is combined atomic number of Ga and N and ρ is density in gm cm^{-3}. From this equation, energy from the beam is nominally being deposited 690 nm into the sample at beam energy 10 keV and 2.2 µm into the sample at 20 keV, over three times the depth of a 10 keV beam. The nominal scanned area at 15 kx magnification was estimated as 4 µm x 2.8µm. This gives an interaction volume of around 7.73 μm^3 and 24.6 μm^3 for 10 keV and 20 keV beam energy respectively. Understanding these parameters is crucial since they describe the nominal interaction volume, where the charge is nominally deposited and the space charge region starts nucleating upon electron beam bombardment. This will be useful in section C, when the volume over which charge has effectively been injected into is discussed, along with the likelihood of charge being either trapped at impurities or stored interstitially. Next section discusses the kinematics associated to both charge injection and luminescence.

B. Time Constants and Dynamic Behaviour of the Space Charge Region

1. *Time Constants,* τ_{CL} and τ_{SC}

Both CL and SC curves were fit to exponential decay curves:

$$y = y_o + A_1\, e^{-\left(\frac{t-t_o}{\tau}\right)} \qquad (5)$$

No constraints were set in the parameters of the equation and values of A_1, τ, and t_0 were varied. The parameter t_o was introduced in the fitting equation in order to optimize the fit. Iterations were run to minimize the χ^2 value for values of time larger than x_o.

Time constants for CL and SC, τ_{CL} and $\tau_{SC,}$ respectively, were plotted for different magnifications, beam currents and beam energy settings, as shown in Fig.3 and 4. Examination of τ_{CL} in Fig.3, reveals a monotonic decrease for increasing magnifications at both 10 and 20 keV. In addition, CL signal decays faster for 10 keV than for 20 keV beam voltage. At all magnifications and beam currents for both beam voltages, a shorter time constant is observed with a faster onset time, that is, time to maximum CL value.

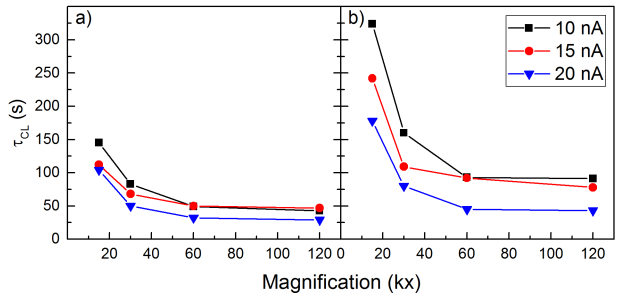

FIG. 3. Time Constants of CL Relaxation at Varying Magnification, (a) 10 keV and (b) 20 keV.

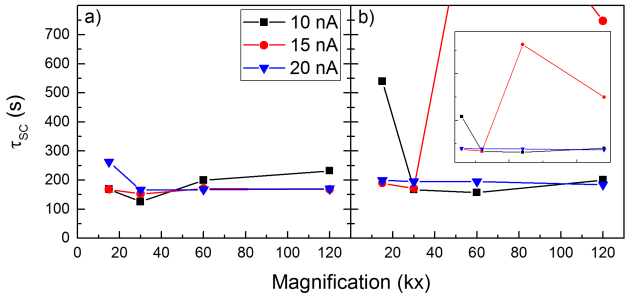

FIG. 4. Time Constants of SC Evolution at Varying Magnification (a) 10 keV and (b) 20 keV, inset of (b) shows full graph.

However, analysis of τ_{SC} in Fig.4 does not show a monotonic dependence on magnifications or beam currents, where time constants at 10 keV are between 100 s and 300 s, and at 20 keV values of τ_{SC} are about 200 s for most experimental conditions, although reaching up to 1300 s at intermediate currents. These results point to the germane message in this work; that of a lack of clear correlation between τ_{CL} and τ_{SC}. Moreover, trends of τ_{CL} are very systematic, whereas τ_{SC} do not vary systematically with experimental conditions. No correlation between τ_{SC} and experimental parameters could be found by ananlyzing the trends in Fig. 4. The systematicity found in τ_{CL} has enabled a parametric description with respect to the experimental parameters, as shown in SI.

Similarly, no correlation between SC evolution to steady state and experimental parameters could be found by analyzing trends in Fig. S4. However, parameteric equations describing the correlation between CL evolution to steady state and experimental parameters could be found by analyzing the trends in Fig. S4, as discussed in SM.

2. *Stored Charge at Steady State*

a. Time-dependent charge injection at steady state SC values

Charge injected at steady state was calculated from measured $i_{sc}(t)$ data for all scans in Fig.1 through the graphical procedure described in the Appendix; and results are shown in Fig.5. For 10 keV, Fig. 5(a), stored charge in the scanned region decreases when magnification is changed from 15 kx to 30 kx. At larger magnifications, stored charge is seen to increase, decrease or not vary. Stored charge values for 10 keV data range from 80 to 400 x 10^{-8} C. For 10 keV data, steady state was reached within irradiation time in all cases. Except for 120 kx magnification, stored charge also increased with beam current. Higher beam current will increase the injection capacity into the sample as higher internal fields will encourage diffusion of trapped charge beyond the interaction volume. In this scheme, under higher beam energies electrons might be injected interstitially in the GaN lattice.

For 20 keV, Fig. 5(b), behaviour of stored charge with scanned region is complex. Stored charge decreased with smaller scanned area for 10 nA beam current and varied little for 20 nA scans despite increasing magnification. Likewise for 15 nA upon 1,000 s irradiation. However, saturation values were much higher at 60 kx and 120 kx magnifications. For 20 keV data, steady state was reached for most cases, except for 15 nA at 60 kx and 120 kx magnifications. These settings, 15 nA 20 keV, provided τ_{SC} larger than average in the specimen current fits at 60 kx, see Fig. 3(b), τ_{SC} is six times larger and at 120 kx three times larger than the 20 nA fit. In these two cases, both stored charge during irradiation time and stored charge at steady state were calculated. Stored charge during

irradiation is half that at steady state for 60 kx and three quarters steady state value at 120 kx magnification. With the exception of these two data points, stored charge values for 20 keV data range from 100 to 400 x 10^{-8} C.

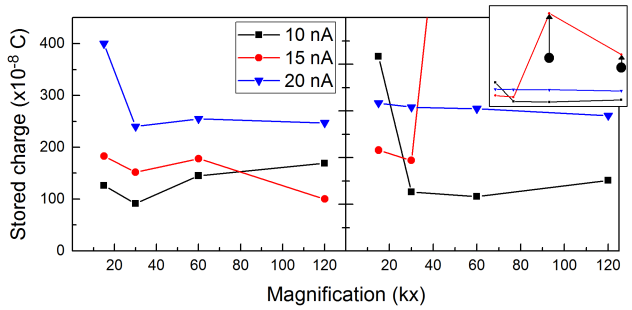

FIG. 5. Steady State Stored Charge at (a) 10 keV and (b) 20 keV Beam Energy. Inset in (b) shows complete graph, up to 1500 x10^{-8} C, with charge measured after 1000 s shown by black circles.

The implications of quantifying total injected charge are key in this study. By estimating the interaction volume of experiments to be 7.7 μm^3 at 10 keV and 15 kx magnification; and assuming a volume of 10 $Å^3$ per atom, there will be 7.7x10^9 atoms in the interaction volume. It is known that the number of electrons trapped within the sample is 8x10^{12} from the stored charge measured at steady state, ~130x10^{-8} C. If this stored charge were exclusively confined to interaction volume alone, each atom within the volume would have to trap 1,000 electrons. From this analysis it is evident that trapped electrons are not confined to the interaction volume. And in fact, storage of one extra electron in 1,000 atoms would be a physically reasonable result, for which the stored charge would need to spread beyond the nominal interaction volume and into the sample, reaching up an effective interaction volume of 8x10^6 μm^3 or 0.01 mm^3. These results resonate with earlier findings reporting SE and CL degraded signals beyond the scanned region due to internal charge dynamics.[14]

The steady stored charge values in Fig. 5 mostly vary between 150 and 300 10^{-8} C for both 10 and 20keV in all these samples in such a way that cannot explain the τ_{CL} or I_{CLSS} progression in Figures 2 and 4 respectively. These findings seem to reinforce the notion that the "direct effects from stored charge", as defined in the Introduction, are not responsible for degraded NBE CL emissions. However, a question arises per the synchronicity between electrical and optical processes. Perhaps the evolution of internal charge dynamics requires examining stored charge at earlier times than the steady state, since both processes, CL and SC could be unfolding within different time scales altogether. Next section will examine the dynamics of charge storage during time.

b. Time-dependent charge injection at short irradiation times

In this section, injected charge prior to the steady state is calculated from Eq. (S3) in SI to examine the dynamics of the space charge region build-up over time. Charge injection at shorter irradiation times was investigated to verify if a pattern of charge dynamics emerges in early stages of irradiation that could cause NBE degradation. Charge injected upon 100, 50 and, 10 s irradiation is shown in Fig. 6. Even when short irradiation times are considered, analysis of Q(t) in Fig.6 shows similar dynamic behaviour to that in Fig. 5 for both 10 keV and 20 keV for all time regimes, still maintaining a dissimilarity with respect to CL dynamics in Fig. 3.

Indeed, the amount of stored charge at 100, 50, and 10 seconds is surprisingly comparable for both irradiation energy and current conditions. In this scheme, stored charge at 20 nA upon 100 s irradiation (Fig.6a) is approximately 120×10^{-12} C, in both 10 and 20 keV settings. This confers an electric field intensity in the 10 keV irradiated regions three times stronger than in the 20 keV region by virtue of nominal irradiation volumes described in section A. However, the τ_{CL} associated to 20 keV are systematically twice the τ_{CL} associated to 10 keV irradiations, suggesting once more the lack of correlation between direct e-beam and decreased NBE processes. A clarification is needed here that, correcting for self-absorption, the generation of NBE CL signals are estimated at 0.5 and 1.5 μm at 10 and 20 keV respectively.[30] Since they still keep a three fold, similarly to the R_{KO} ratio at both energies, the arguments respect to the influence of the space charge region on the NBE dynamics, hold regardless whether the nominal interaction volume or the volume that is being effectively sampled through NBE CL is considered.

Finally, it is worth highlighting that the stored charge at steady state do show a consistent description of the charge build up process at 10 keV, since the graphs shown in Fig. 6 overall keep similar trends to those in Fig. 5. At 20 keV, the detail seen at the shorter irradiation times, with more steady evolution at different magnifications, still fail to explain the evolution of τ_{CL} with magnification. For example, by comparing the stored charge to magnification in Fig. 6c, a systematic ratio of 1 for all currents is obtained. However, ratios in τ_{CL} amount to 1 only in the highest magnifications, and lower magnifications see a difference of two and three fold for 10 and 20 nA respectively.

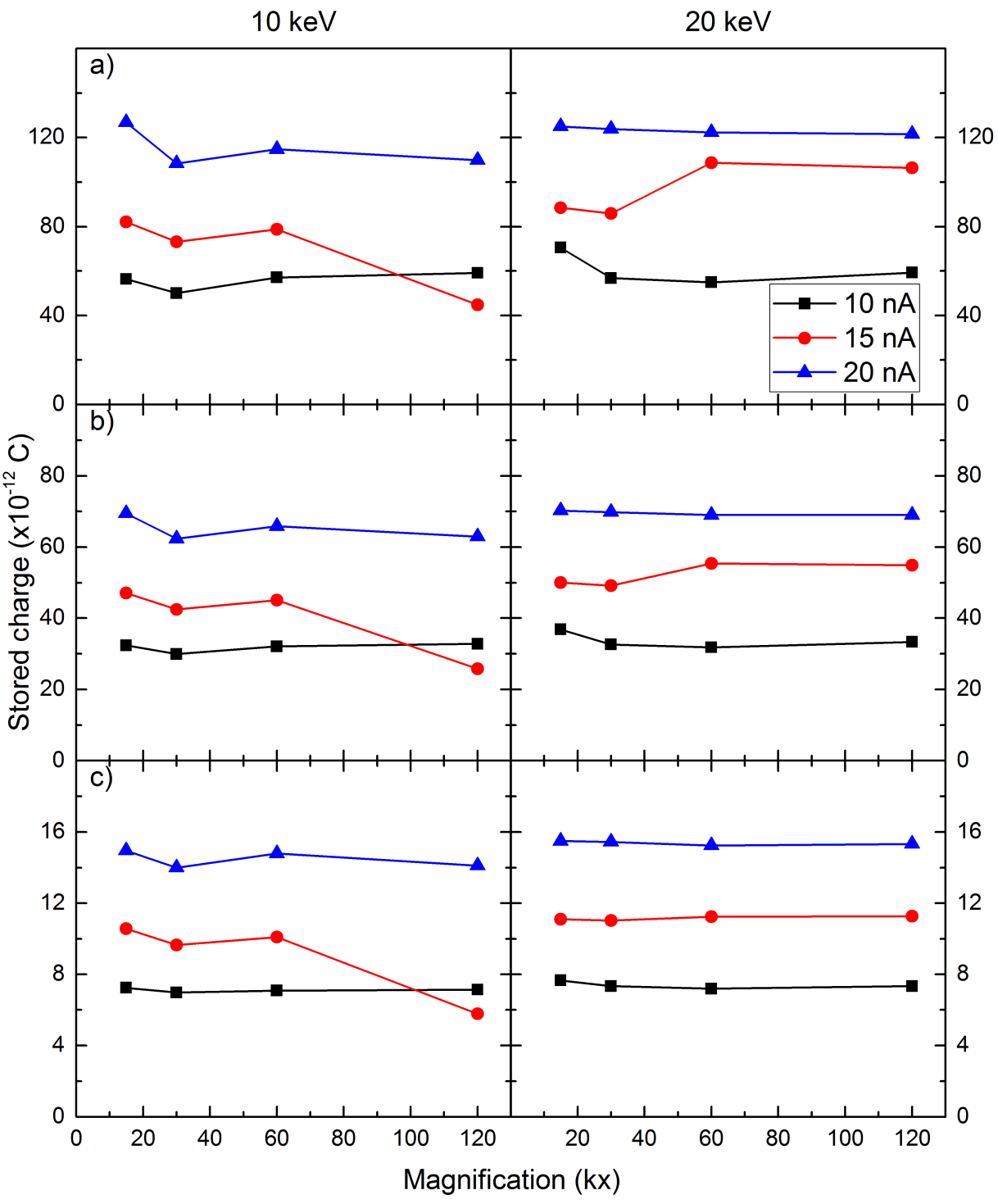

FIG. 6. Charge storage as a function of magnification; (a) 100 s, (b) 50 s and (c) 10 s irradiation. Graphs on the left hand side show irradiation at 10 keV and on the right analogous experiments at 20 keV.

C. Time-dependent injected charge and cathodoluminescence: a model for V_G activation dominating CL emission over charge trapping

Summarizing, in section 2a) comparison between trends of steady state stored charge and τ_{CL}, suggested that direct effects from stored charge (i.e. e-h generation rate and recombination efficiency through internal built-in fields) were not dominating CL intensity progression. A scenario where a variety of processes would be igniting at different time frames during the space charge built up process was then considered. Examination of earlier time frames, prior to the steady state examined in 2a), was conducted in section 2b). It was found that, despite some commonalities in saturation behaviour, overall trends of early stored charge did not follow τ_{CL} trends, the former featuring crossover and inconsistent gradients that were not reciprocated by the latter. The non-monotonic current dependence in Figures 5 and 6 suggest that there is indeed interplay between stored charge and defect activation as factors that affect luminescence. Given the monotonic behavior of τ_{CL}, this suggests that stored charge is not a primary factor compared with defect activation throughout the irradiation period

Moreover, these results suggest that mechanisms resulting from direct electric field build up, are not responsible for decreased CL signals at early stages. If built-in electric fields are not affecting direct e-h generation or recombination efficiency, and since decreased signals appear within seconds of irradiation therefore making electromigration an improbable factor, the decreased CL signals at early stages are attributed to the activation of traps under electron beam bombardment, in agreement with findings by Nykanen et. al. [5,12] As described earlier in Section 1, they attributed decreased NBE CL signals upon low energy beam irradiation to the activation of V_{Ga} by virtue of hydrogen desorption of the trivalent associated complex.[5] And in fact, these are common defects in GaN, that, at a time, were candidates to DL emissions,[31] and whose concentrations have been estimated in the order of 10^{-16} cm^{-3}.[11] Within this experimental set up, a scenario using 10keV, 15kx magnification was considered, that provides a nominal irradiation volume of 7.7 μm^3, for which a steady state stored charge of $8x10^{12}$ electrons was calculated, which will be available to fill about 2.6 $x10^{12}$ activated $V_{Ga.}$. Since there are only $8*10^4$ V_{Ga} available in the nominal interaction volume, it can be assumed, that, statistically, all are likely to be filled, and excess charge is being either injected interstitially (i.e. increasing the GaN's electron carrier density in the region irradiated by the electron beam) or diffusing beyond the nominal interaction volume, as discussed in Section 2a.[14]

The impact of stored charges in NBE CL degradation has not been taken into account in the original discussion by Nykanen *et al*.[5] However, the large amount of stored charge readily available in the nominal interaction volume

and beyond (i.e. the space charge region) needs to be taken into account to fully explain CL evolution at later irradiation stages, once the space charge region is established.

Indeed, in this model it is proposed that (Fig. 7) electron-beam activated traps develop already at early irradiation stages, (step 1 in Fig. 7) and those dominate CL decay (step 2 in Fig. 7). Also for this reason, V_{Ga} are likely to be activated primarily upon knock-on damage at very earlier stages and by current density effects later, as the space charge region gets established.[5,14] Indeed, $V_{Ga.}$ got activated to decrease NBE CL intensities to a steady-state (step 3 in Fig. 7). Different experimental settings had an impact on how the kinetics of the trap filling process unfolded, with shorter time constants for higher currents, higher magnifications and lower energies, as expected. The CL time constant τ_{CL} has been parametrically described as a function of the experimental parameters in SM. In this scheme, additional available electrons go on as interstitials to make up the space charge region, (step 4 in Fig. 7) extending well beyond that of the nominal irradiation region as discussed in section 3a and in earlier works.[14] Importantly, once V_{Ga} have been filled, the space charge region (beyond the nominal interaction volume) becomes the main actor in trying to maintain the steady state, with a steady generation and recombination of electron hole pairs at the NBE. In this stage, the space charge region is having a direct impact on the generation and recombination of electron home pairs.

Finally, a brief discussion is needed on the possibility of impurity electromigration. It is through diffusion currents derived from the steady state that electromigration of existing impurities (V_N, C_N, etc…) could also have an impact on NBE CL. However, DL CL had been shown invariant under irradiation, [14,18] and current theories point at C_N as possibly responsible for the DL emissions, suggesting that C_N has not electromigrated. This results suggests that electromigration of impurities within the space charge region are unlikely, perhaps due to the high presence of threading dislocations in the window region of LEO-GaN, that could effectively anchor these point defects.

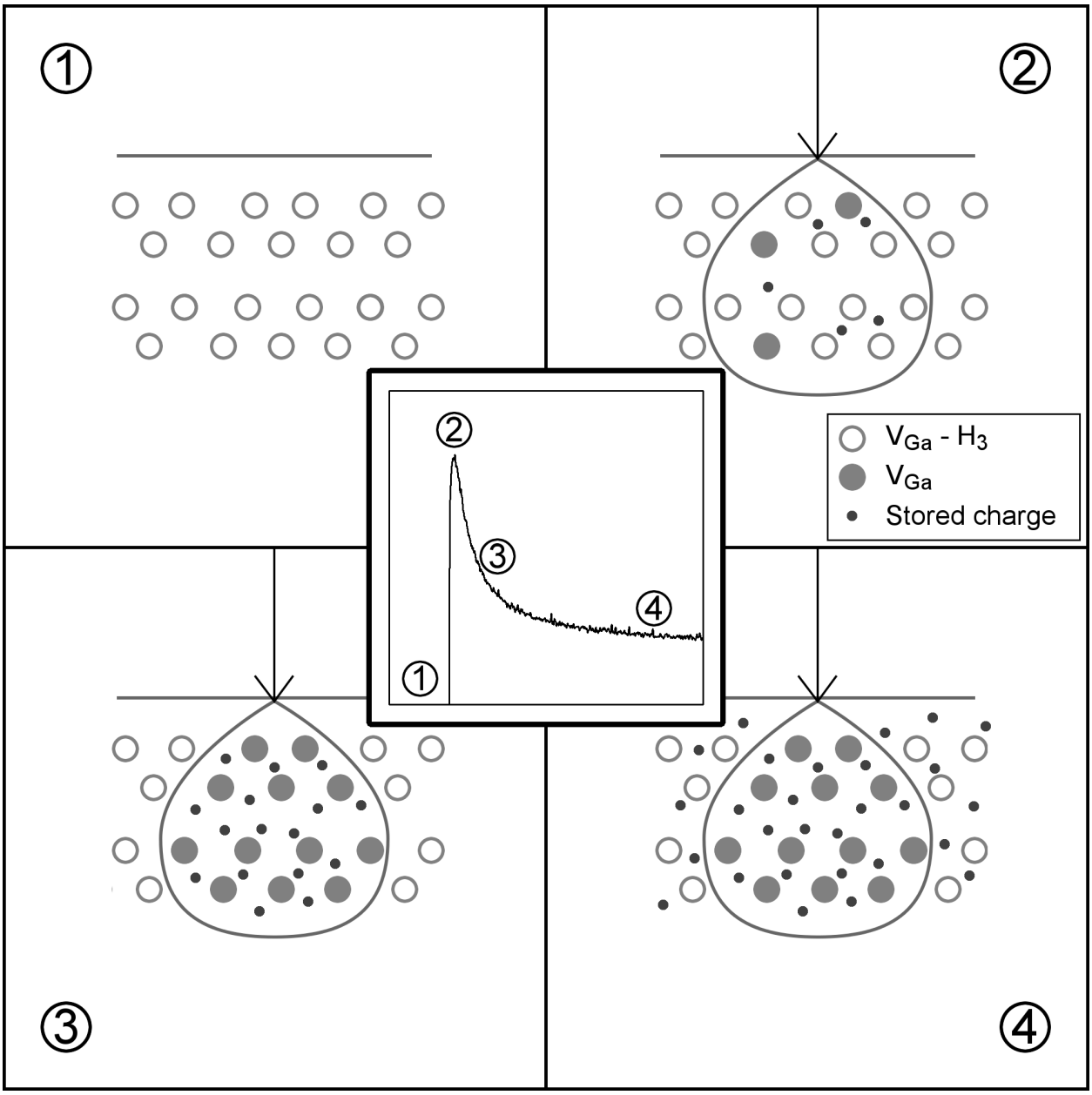

FIG. 7. Correlation between charging dynamics and NBE CL, with the nominal interaction volume being enclosed within the circle and final space charge region extending beyond it. (1) Prior to beam irradiation, V_{Ga} complexes are inactive, there is no stored charge and the interaction volume has not been defined. (2) Upon beam on, V_{Ga} activate to yield non-radiative centers, and some charge is being stored in the nominal interaction volume. As a consequence, diffusion currents start to flow with some contribution to the incipient decay of NBE CL signal. (3) Upon prolonged irradiation, all V_{Ga} have been activated and stored charge has saturated in the nominal interaction volume. (4) Leakage currents promote further injection beyond the nominal interaction volume. The equilibrium between the activated V_{Ga} lattice and the space charge region, is responsible for the steady state NBE CL emissions.

IV. CONCLUSIONS

In this work, a model was developed to explain dynamics behind optoelectronics devices, such as lasers and LEDs, that operate at high current density, and their degradation by monitoring the in situ evolution of electrical and optical signals. Using momentary current density values analogous to those in operational devices, NBE CL was found to decrease systematically with experimental parameters. SC dynamics were found to be more erratic, and both were difficult to correlate. This poor correlation led to the conclusion that direct space charge effects (by way of affecting generation or recombination efficiency of electron-hope pairs) are not the main actors at early irradiation stages. The NBE CL dynamics discussed here is mostly due to knock-on beam effects through the activation of pre-existing V_{Ga}, which are responsible for CL quenching at early irradiation stages. At later irradiation stages, direct and indirect effects will likely contribute to the CL degradation and steady state. Direct effects will modulate electron-hole generation and recombination, and indirect effects will also contribute to the activation of V_{Ga}, which did not result in additional CL emissions. Calculation of the steady state stored charge offered evidence that the space charge region extends beyond the nominal interaction volume. At later irradiation times, the equilibrium between the filled V_{Ga} lattice and the space charge region is responsible for the steady state NBE CL intensities. It is still uncertain if V_{Ga} beyond the nominal interaction volume can be activated through diffusion currents or whether these traps can be restored to its original V_{Ga}-3H complex. This restoration process could perhaps follow from annealing or beam off conditions. It is not clear either what the role is of the desorbed atomic hydrogen from the nominal vacancy complexes or if it can resorb. However, elucidation of these phenomena could offer solutions to aging laser diodes, besides the obvious, growth of GaN systems with fewer V_{Ga}.

SUPPLEMENTARY MATERIAL

See supplementary material for a complete description of the Song's model and additional supporting discussion.

ACKNOWLEDGMENTS

The authors gratefully acknowledge scientific discussions with G. Slade Cargill III.

V. REFERENCES

[1] S. Pimputkar, J. S. Speck, S. P. DenBaars, and S. Nakamura, Nat. Photonics **3** (4), 180 (2009); I. T. Ferguson, A. Melton, T. Xu, M. Jamil, and W. Fenwick, Published in the Proceedings of SPIE Optical Engineering+ Applications, 77840A (2010); M. Pavesi, F. Rossi, and E. Zanoni, Semicond. Sci. Technol. **21** (2), 138 (2006); A. Mukhtarova, S. Valdueza-Felip, L. Redaelli, C. Durand, C. Bougerol, E. Monroy, and J. Eymery, Appl. Phys. Lett. **108** (16), 161907 (2016).

[2] R. Belkorissat, O. Jbara, S. Rondot, N. Benramdane, M. Belhaj, and A. Hadjadj, Meas. Sci. Technol. **24** (5), 055902 (2013); G. B. Feng, M. Cao, L. P. Yan, and H. B. Zhang, Micron **52**, 62 (2013); Y. Xu, O. T. Hofmann, R. Schlesinger, S. Winkler, J. Frisch, J. Niederhausen, A. Vollmer, S. Blumstengel, F. Henneberger, N. Koch, P. Rinke, and M. Scheffler, Phys. Rev. Lett. **111** (22), 226802 (2013); J. Cazaux, J. Appl. Phys **85** (2), 1137 (1999); J. Cazaux, J. Appl. Phys. **111** (6), 064903 (2012).

[3] M. Meneghini, S. Carraro, G. Meneghesso, N. Trivellin, G. Mura, F. Rossi, G. Salviati, K. Holc, T. Weig, L. Schade, M. A. Karunakaran, J. Wagner, U. T. Schwarz, and E. Zanoni, Appl. Phys. Lett. **103** (23), 233506 (2013).

[4] M. J. Wallace, P. R. Edwards, M. J. Kappers, M. A. Hopkins, F. Oehler, S. Sivaraya, D. W. E. Allsopp, R. A. Oliver, C. J. Humphreys, and R. W. Martin, J. Appl. Phys. **116** (3), 033105 (2014).

[5] H. Nykänen, S. Suihkonen, L. Kilanski, M. Sopanen, and F. Tuomisto, Appl. Phys. Lett. **100** (12), 122105 (2012).

[6] A. Y. Polyakov, D. W. Jeon, I. H. Lee, N. B. Smirnov, A. V. Govorkov, E. A. Kozhukhova, and E. B. Yakimov, J. Appl. Phys **113** (8) (2013).

[7] A. Y. Polyakov, S. J. Pearton, P. Frenzer, F. Ren, L. Liu, and J. Kim, Journal of Materials Chemistry C **1** (5), 877 (2013).

[8] M. Amilusik, T. Sochacki, B. Lucznik, M. Fijalkowski, J. Smalc-Koziorowska, J. Weyher, H. Teisseyre, B. Sadovyi, M. Bockowski, and I. Grzegory, J. Cryst. Growth **403**, 48 (2014).

[9] M. A. Reshchikov and H. Morkoc, J. Appl. Phys **97** (6), 061301 (2005).

[10] L.-Q. Liu, M. Eder, I. Burgert, D. Tasis, M. Prato, and H. D. Wagner, Appl. Phys. Lett. **90** (8), 083108 (2007).

[11] C. G. Van de Walle and J. Neugebauer, J. Appl. Phys. **95** (8), 3851 (2004).

[12] H. Nykänen, S. Suihkonen, T. Tanikawa, M. Yamaguchi, Y. Honda, and H. Amano, Physica Status Solidi (A) **210** (2), 383 (2013).

[13] P. Sherwood, J. Electron Spectrosc. Relat. Phenom. **176** (1–3), 2 (2010).

[14] E. M. Campo, M. Pophristic, L. Hopkins, and I. T. Ferguson, Appl. Opt. **54** (12), 3613 (2015).

[15] M. Toth, M. R. Phillips, J. P. Craven, B. L. Thiel, and A. M. Donald, J. Appl. Phys. **91** (7), 4492 (2002).

[16] M. A. Stevens-Kalceff and K. J. Levick, Microscopy Research and Technique **70** (3), 195 (2007).

[17] G. Pozina, P. P. Paskov, J. P. Bergman, C. Hemmingsson, L. Hultman, and B. Monemar, Appl. Phys. Lett. **91** (22), 1 (2007).

[18] E. M. Campo, G.S. Cargill III, M. Pophristic, I. Ferguson, MRS Int. J. Nitride Semicond. Res. **09** (08) (2004).
[19] Y. El Gmili, G. Orsal, K. Pantzas, T. Moudakir, S. Sundaram, G. Patriarche, J. Hester, A. Ahaitouf, J. P. Salvestrini, and A. Ougazzaden, Acta Mater. **61** (17), 6587 (2013).
[20] J. Joh and J. A. Del Alamo, presented at the Electron Devices Meeting, 2006. IEDM'06. International, 2006 (unpublished).
[21] M. Meneghini, A. Tazzoli, G. Mura, G. Meneghesso, and E. Zanoni, Electron Devices, IEEE Transactions on **57** (1), 108 (2010).
[22] M. T. Hardy, D. F. Feezell, S. P. DenBaars, and S. Nakamura, Materials Today **14** (9), 408 (2011).
[23] M. Xiao, J. Zhang, X. Duan, H. Shan, T. Yu, J. Ning, and Y. Hao, Scientific Reports **6**, 23842 (2016).
[24] T. Hamaguchi, N. Fuutagawa, S. Izumi, M. Murayama, and H. Narui, presented at the SPIE Gallium Nitride Materials and Devices XI, 2016 (unpublished).
[25] J. Song, G. Yuan, K. Xiong, B. Leung, and J. Han, Cryst. Growth Des. **14** (5), 2510 (2014).
[26] Z. G. Song, C. K. Ong, and H. Gong, J. Appl. Phys **79** (9), 7123 (1996).
[27] E. J. Vesseur, T. Coenen, H. Caglayan, N. Engheta, and A. Polman, Phys. Rev. Lett **110** (1), 013902 (2013); L. Hussey, S. Mita, J. Xie, W. Guo, C. R. Akouala, J. Rajan, I. Bryan, R. Collazo, and Z. Sitar, J. Appl. Phys **112** (11) (2012).
[28] J. K. Hsu, T. Y. Lin, C. Y. Lai, T. C. Chien, J. H. Song, and P. H. Yeh, Appl. Phys. Lett. **103** (12), 3 (2013).
[29] J. Goldstein, *Scanning Electron Microscopy and X-ray Microanalysis: Third Edition*. (Springer US, 2003).
[30] K. Fleischer, M. Toth, M. R. Phillips, J. Zou, G. Li, and S. J. Chua, Appl. Phys. Lett. **74** (8), 1114 (1999).
[31] J. L. Lyons, A. Janotti, and C. G. Van de Walle, Appl. Phys. Lett. **97** (15) (2010); J. Neugebauer and C. G. Van de Walle, Appl. Phys. Lett. **69** (4), 503 (1996).